Cloning and trapping of magnetostatic spin-wave pulses by parametric pumping

Kevin R. Smith,[1] Vitaliy I. Vasyuchka,[1,2] Mingzhong Wu,[1] Gennadiy A. Melkov,[2] and Carl E. Patton[1]
[1]*Department of Physics, Colorado State University, Fort Collins, Colorado 80523, USA*
[2]*Faculty of Radiophysics, National Taras Shevchenko University of Kiev, Kiev 01033, Ukraine*
(Received 4 October 2006; revised manuscript received 16 February 2007; published 6 August 2007; corrected 16 August 2007)

Magnetostatic backward volume spin-wave (SW) pulses have been cloned and trapped through the use of multiple, properly timed, parametric pumping (PP) pulses. The experiment was done with 30-ns-wide pulses at 5 GHz in a 7.1-μm-thick yttrium iron garnet film. Well-timed, large-area, high-power, 2-ns-wide microwave pulses at 10 GHz were used to pump the SW pulses. The interaction between the initial SW and PP pulses created a mirror-image, time-reversed idle SW pulse with the same frequency as, but opposite wave vector to, the initial SW pulse. Additional properly timed PP pulses continued the reversal process and yielded exact clones of the original SW pulse. The relative peak output powers of the clone pulses could be adjusted through changes in the pumping power.

DOI: 10.1103/PhysRevB.76.054412 PACS number(s): 76.50.+g, 75.30.Ds, 85.70.Ge

I. INTRODUCTION

Recent work on three-wave parametric interactions has revealed a variety of new nonlinear effects for a range of different physical systems. This work includes escape from self-trapping in a double-well potential in Bose-Einstein condensate systems[1] and entangled quantum states,[2] parametric light generation in nonlinear optical media,[3] phase noise reduction in crystal oscillators,[4] theoretical production of neutrino-antineutrino pairs in degenerate dense plasmas,[5] and momentum reversal in magnetic thin films.[6] This paper describes the use of three-wave parametric processes to produce actual clones of propagating wave packets in nonlinear media. The specific work was done for 5 GHz magnetostatic spin-wave pulses in a single-crystal yttrium iron garnet (YIG) thin film. It was possible to produce up to two wave packet clones from a single input pulse. In essence, the cloning process derives from a sequence of time-reversed pulse operations induced by parametric pumping.[7] The pulse cloning process demonstrated here can be applied to any physical system that can support three-wave parametric processes. The sections that follow present the method, qualitative theoretical foundations, and selected details of the experiment, and give key results.

II. THE CLONING PROCESS

Figure 1 shows the experimental cloning assembly. One starts with a long and narrow single-crystal YIG film strip with input and output transducers, as indicated. An external static uniform magnetic field is applied parallel to the long direction of the YIG film strip. This field-film geometry corresponds to the magnetostatic backward volume wave (MSBVW) spin-wave propagation configuration.[8] An open dielectric resonator (ODR) structure is positioned to enclose the central portion of the YIG strip. The part of the YIG strip inside the ODR element comprises the parametric pumping region for the cloning process. The purpose of the ODR element itself is to couple the pumping power, taken as P_{pump}, to the signal pulse.

In brief, the cloning process occurs as follows. (1) A microwave signal pulse at some carrier frequency ω_s, is applied to the input transducer. (2) This input pulse produces a propagating spin-wave pulse in the YIG strip. (3) A series of properly timed and narrow microwave pulses at some different frequency ω_p is then applied to the ODR structure while the spin-wave pulse is *inside* the parametric pumping region. The diagram shows two such pulses, labeled $P1$ and $P2$. (4) Under appropriate conditions, one then realizes two output pulses, an amplified signal pulse labeled as S' in Fig. 1, and a cloned pulse labeled as C. One can use more pumping pulses to produce additional clones.

Figure 2 shows a sequence of diagrams that demonstrate the cloning process. The diagrams do not take dispersion, decay, or amplification of the pulses into account. The light gray bars indicate the part of the YIG strip that is inside the ODR element. The S, S', R, R', and C labels identify the

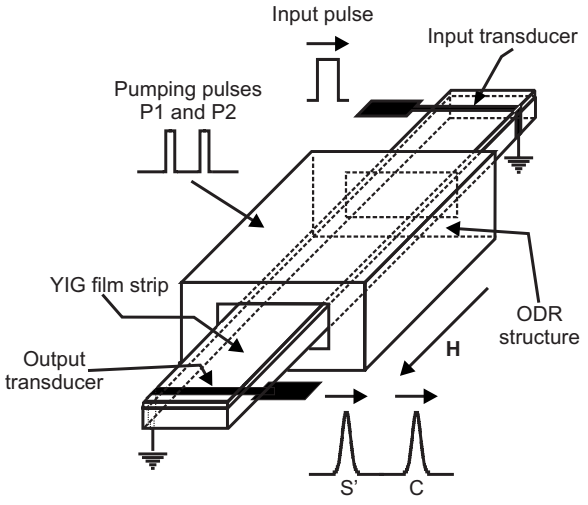

FIG. 1. Spin-wave excitation, propagation, and pumping assembly. The yttrium iron garnet (YIG) film strip is centered within the open dielectric resonator (ODR) structure. A static magnetic field **H** is applied parallel to the strip. Input and output transducers couple pulse power into the YIG strip and detect the generated spin-wave pulses at the output, as indicated. Parametric pumping occurs through the application of pulses $P1$ and $P2$ to the ODR structure. Amplified and cloned pulses, S' and C, respectively, are detected at the output.

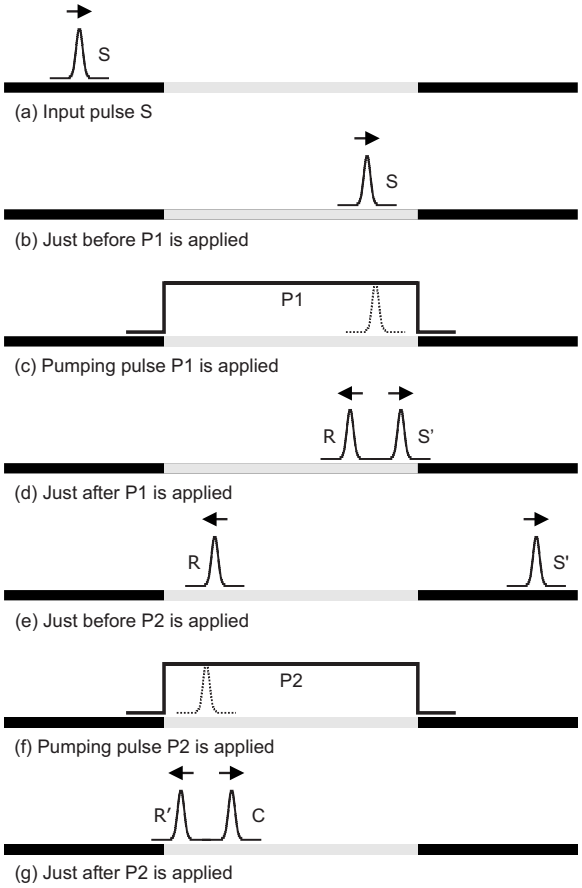

FIG. 2. Schematic layout of the cloning process. The panels show snapshots of the spin-wave pulses S, S', R, R', and C, as well as the pumping pulses $P1$ and $P2$, at different times. The black and gray bar represents the yttrium iron garnet (YIG) film strip. The light gray segments indicate the portions of the YIG strip that are inside the open dielectric resonator structure. The arrows show pulse propagation directions.

spin-wave pulses at various points in time and space along the YIG strip. Right-pointing arrows above the pulses indicate propagation away from the input transducer, and vice versa. Figures 2(c) and 2(f) also show the ODR pumping pulses $P1$ and $P2$, as well as the spin-wave pulse inside the pumping region, just at the time the pumping pulse is applied.

The sequence of events in Fig. 2 is as follows. One starts with the initial right-propagating spin-wave pulse S, as in Fig. 2(a). The pulse moves into the ODR region, as in Figs. 2(b) and 2(c). The short parametric pumping pulse $P1$ is applied when S is near the right end of the ODR region, as in Fig. 2(c). Figure 2(d) shows the effect of $P1$ on S. One now has a right-traveling signal pulse S' and a new left-traveling idle, or reversed, wave pulse R. Figure 2(e) shows the pulse S' as it moves out of the pumping region and the reversed pulse R as it moves toward the left end of the structure. Pulse R is now in position for the application of the second pumping pulse $P2$, as in Fig. 2(f).

The second parametric pumping pulse has the same effect on R that $P1$ had on S. One then obtains a left-traveling pulse R' and a right-traveling idle pulse C, as in Fig. 2(g). The label C emphasizes that this second reversed pulse is a *clone* of the original pulse S. In brief, the combination of the single input pulse and the two parametric pumping pulses gives (1) an amplified signal pulse S' and (2) a "cloned" pulse C after a substantial trapping delay. Additional clones may be produced through a repeat of the parametric pulse sequence in Figs. 2(c) and 2(f). In later sections, data will be shown for the production of two clones.

III. THE THREE-WAVE PARAMETRIC INTERACTION

The creation of the reversed pulses R and C in Fig. 2 derives from a three-wave parametric interaction between the electromagnetic pumping pulse $P1$ and the magnetostatic spin-wave pulse S, or between $P2$ and R. The properties of the new reversed pulses are determined by basic energy and momentum conservation considerations.

Each signal pulse has an energy $\hbar\omega$, where $\hbar$ is Plank's constant. If one sets the pumping pulse frequency ω_p equal to *twice* ω_s, the energy conservation condition $\omega_p=\omega_s+\omega_i$, where ω_i is the idle pulse frequency, forces the carrier frequencies of all subsequent idle and clone pulses to ω_s.

Similarly, each pulse has a momentum $\hbar\mathbf{k}$. The wave vectors of the pumping pulse, the input signal pulse, and the idle pulse are $\mathbf{k}_p$, $\mathbf{k}_s$, and $\mathbf{k}_i$, respectively. The length L of the ODR pumping region sets $|\mathbf{k}_p|$ at $2\pi/L$. The signal pulse wavelength λ_s is much shorter than L. This corresponds to the wave vector condition $|\mathbf{k}_p| \ll |\mathbf{k}_s|$. As a result, the general momentum conservation condition $\mathbf{k}_p=\mathbf{k}_s+\mathbf{k}_i$ reduces to the simpler condition $\mathbf{k}_i \approx -\mathbf{k}_s$.

From the above, one can see that a pumping pulse at $\omega_p=2\omega_s$, in combination with an extended pumping region, always gives a reversed spin-wave pulse with the same frequency and same wave number as the input signal pulse. This reversal takes place every time a pumping pulse is applied to a spin-wave pulse inside the ODR region. It is important to note that the pulses that result from the reversal process in each case are phase conjugated or time reversed.[7]

There is one caveat to the above scenario. In order to maintain the shape of the original input spin-wave pulse, the temporal width τ_p of the pumping pulse must be much narrower than that of the spin-wave pulse, τ_s.[9] Ideally, the pumping pulse should be in the form of a δ function. In practice, the condition $\tau_p \ll \tau_s$ is generally sufficient to ensure a clean reversed pulse.

The schematic frequency vs wave vector diagram in Fig. 3 illustrates the three-wave parametric interaction and the energy and momentum conservation constraints that govern the spin-wave pulse reversal process described above. The graph shows two MSBVW dispersion curve branches for oppositely directed wave vectors, shown in one dimension and written in terms of wave number as $\pm k$. The diagram also shows three schematic spin-wave pulse profiles. The solid circles denote the corresponding frequency–wave-number operating points for these signals. The large arrows show the action of the parametric pumping pulse $P1$ on pulse S. This action produces the amplified pulse S' and the reversed idle pulse R. With the pumping pulse at $\omega_p=2\omega_s$ and $k_p \approx 0$, one always produces an amplified pulse S' and an idle pulse R at ω_s as well, and $k=\pm k_s$, respectively.

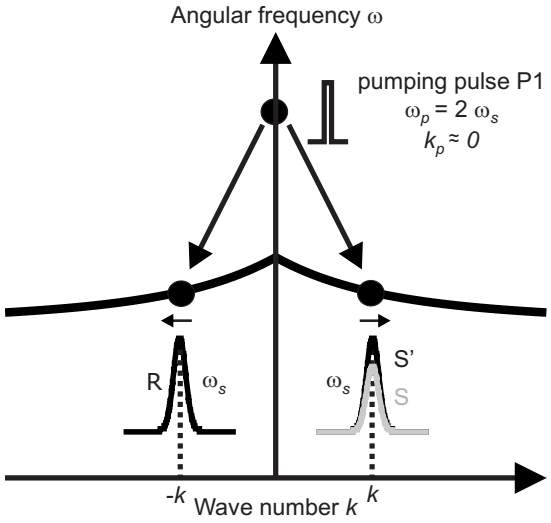

FIG. 3. Schematic illustration of the three-wave parametric process that leads to cloning. The diagram shows the applicable spin-wave dispersion diagram of frequency ω vs wave number k with the pumping pulse $P1$, the signal pulse S, the amplified pulse S', and the idle pulse R at their appropriate operating points, as indicated. The arrows above the pulses show relative propagation directions. The large arrows indicate the power transfer from $P1$ to S to create S' and R.

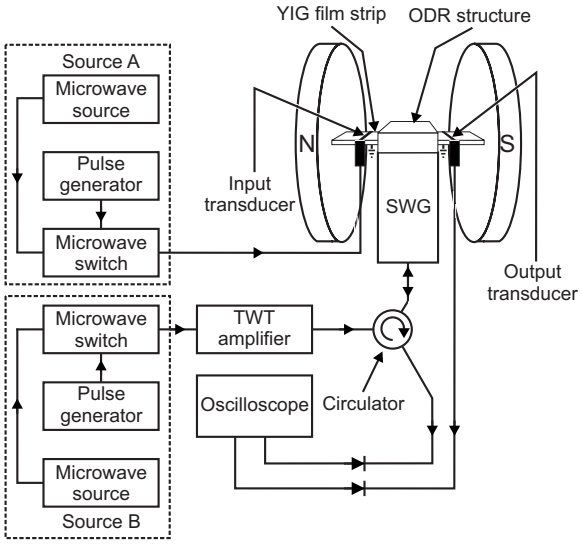

FIG. 4. Schematic diagram of the setup for spin-wave pulse cloning. The microwave structure from Fig. 1 is centered between the pole pieces of an electromagnet. The yttrium iron garnet (YIG) film strip, input and output transducers, and open dielectric resonator (ODR) components are as indicated. Sources A and B, each comprised of a microwave synthesizer, a fast pulse generator, and a microwave switch, provide the input pulse and the parametric drive pulses, respectively. The ODR feed includes a traveling wave tube (TWT) amplifier, a circulator, and a shorted wave guide (SWG). Output pulses and reflected power from the ODR structure are detected and displayed on a fast oscilloscope.

IV. EXPERIMENTAL CLONING SETUP

Figure 4 shows a schematic diagram of the overall experimental setup. The YIG film excitation, propagation, and pumping structure have already been considered in Fig. 1. A nominal 5 GHz microwave pulse from source A applied to the input microstrip line excites the input MSBVW pulse in the YIG strip. A nominal 10 GHz high-power narrow pulse from source B is applied to the ODR structure through a traveling wave tube (TWT) amplifier, a circulator, and a shorted waveguide. Signals from the output transducer and reflected pulse power from the ODR structure are routed to separate diode detectors and the waveforms are monitored with a fast oscilloscope. An electromagnet provides a static uniform magnetic field parallel to the YIG strip that defines the MSBVW propagation mode in the film.

The experiment utilized a 40-mm-long, 7.1-μm-thick, 2-mm-wide low-loss single-crystal YIG film strip. The input and output transducers were 20 μm wide and placed 6 mm apart. The ODR structure was made from a high-density thermostable ceramic block and had a nominal 10 GHz relative permittivity of 80. The structure was 4.2 mm long, 4.1 mm wide, and 2.3 mm thick. Microwave power from the short was coupled to the ODR structure through a standard waveguide flange and a small rectangular hole with the resonator positioned inside. A small metal reflector was also placed on top of the ODR structure. The reflector served to boost the power absorbed by the resonator by about 20 dB.

The microwave sources were each comprised of a cw microwave synthesizer and a microwave switch driven by a fast pulse generator. The pulses from source A were maintained at low power levels and narrow widths in order to avoid nonlinear effects. The pulse generator in source B could produce one, two, or four equal-width delayed pulses for a given trigger. Pulses from the TWT amplifier provided the requisite P_{pump} to the ODR structure. The circulator was used to monitor the reflected power from the ODR structure. The realization of a cloned spin-wave pulse was done in seven steps. (1) *In situ* network analyzer measurements of the ODR response were used to determine the resonant frequency. For the setup given above, $\omega_p/2\pi$ was 9.870 GHz. (2) The position of the metal reflector cap was fine tuned to optimize the coupling of source B power to the resonator. (3) The signal frequency was set to $\omega_s/2\pi=(1/2)(\omega_p/2\pi)=4.935$ GHz. (4) The static magnetic field was adjusted to position the MSBVW cutoff frequency about 50 MHz above the signal frequency. The nominal field for this band position was 1080 Oe and the corresponding operating point MSBVW k_s value was about 120 rad/cm. (5) The width and power of the input signal pulse from source A were set to 30 ns and 20 μW, respectively. These values were large enough to provide useful pulse signals for the trapping and cloning process but small enough to keep all signals and clone pulses in the linear, nonsolitonic regime.[10] (6) The production of MSBVW pulses was verified at the output transducer structure. The output pulse delay time indicated a spin-wave pulse group velocity of 2.9×10^6 cm/s, in good agreement with magnetostatic wave theory.[8] (7) Source B was set to produce two properly timed 10-ns-wide pumping pulses at a power level sufficient to produce a single cloned output pulse, as in Fig. 2. The application of two additional and properly timed pumping pulses from source B produced a second clone pulse. Data

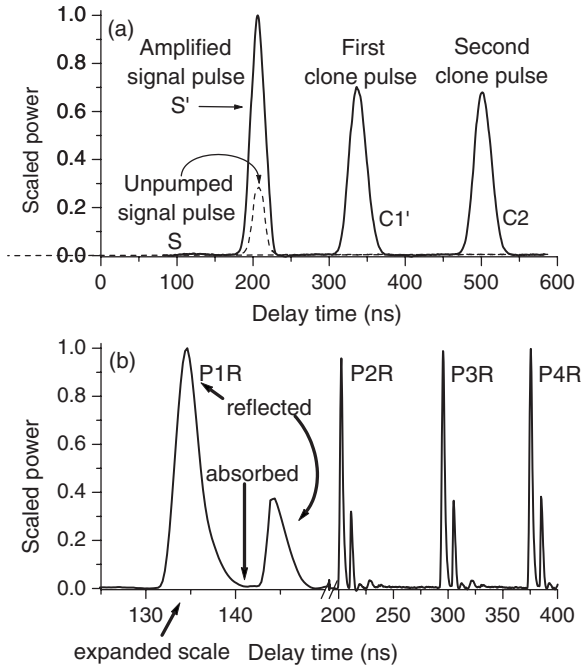

FIG. 5. Representative time traces for (a) the output pulses and (b) the reflected pumping power from the open dielectric resonator (ODR) structure. (a) shows one unpumped output pulse S and three representative output pulses S', $C1'$, and $C2$ obtained for four pumping pulses with the timing as shown in (b). The pumping power was 22.1 W. (b) shows four representative pumping pulse reflections from the ODR structure. Pulse $P1R$ is shown on an expanded time scale.

were also obtained for a range of pumping pulse powers.

V. EXPERIMENTAL CLONING RESULTS

Representative output pulse data are shown in Fig. 5, along with companion data on the reflected P_{pump} from the ODR structure. All time scales are referenced to the launch time of the initial signal pulse S. The pumping power was 22.1 W. For these data, both P_{pump} and the pumping pulse timing were adjusted to give clean clones with comparable amplitudes. Figure 5(a) shows two output power vs time traces. The solid curve is for an input pulse S and four properly timed pumping pulses applied, as discussed above. The dashed curve, shown as a point of reference, is for the same input pulse S, but with no pumping pulses applied. The traces have been normalized to the highest peak. The S, S', $C1'$, and $C2$ labels follow the nomenclature established above. The primes indicate the amplification of the corresponding forward traveling pulse. Figure 5(b) shows the reflected signals from the ODR structure for the four pumping pulses $P1$ through $P4$ that were used to produce the clones shown in Fig. 5(a). These are labeled as $P1R$ through $P4R$. As in (a), these traces have been normalized to the highest peak. The $P1R$ pulse is shown on an expanded scale to illustrate the pulse structure.

The output signal traces in Fig. 5(a) show three things. (1) With no pumping pulses applied, one realizes only an *unamplified* signal pulse S and no cloned pulses. (2) With four pumping pulses applied, one realizes an *amplified* signal pulse S' and two cloned pulses $C1'$ and $C2$. (3) For this particular P_{pump}, the two clones have about the same peak powers, taken as P_{peak}, and are about 70% of the P_{peak} for S'. As will be discussed shortly, one can use the P_{pump} level to control the relative P_{peak} values of the clones. Figure 5(b) shows two things. (1) The reflected signals of the individual pumping pulses are double peaked. (2) The width of the near-zero reflection region of each pulse is on the order of 1–2 ns.

The data in Fig. 5 demonstrate two key points. First, the cloning and trapping process works. If one takes the group velocity of the MSBVW pulses into account, the pumping pulses in Fig. 5(b) give spin-wave pulse locations inside the pumping region, as depicted in Fig. 2. It is clear, then, that action of these pumping pulses gives the amplified pulse S' and clones $C1'$ and $C2$. Second, Fig. 5(b) shows the timing of the pumping pulses that is needed to produce clones. It also shows that the effective pumping pulse widths satisfy the $\tau_p \ll \tau_s$ condition established above. The 1–2 ns widths of the near-zero reflection regions correspond to τ_p. Recall that the overall spin-wave pulse full widths at half maximum are about 30 ns.

As noted above, the clean clone profiles in Fig. 5(a) were a result of a careful setup of the pumping pulses to match the scenario depicted in Fig. 2. Additionally, the nearly equal clone amplitudes is a result of a properly selected P_{pump} level applied to the ODR structure. Changes in either the timing or the peak P_{pump} lead to significant changes in the output profiles. As for timing, as long as the pumping pulses are applied while the signal pulses are inside the pumping region, the clone action is realized according to the Fig. 2 scenario. If the pumping pulses are applied at times when the signal pulses are close to either edge of the ODR structure or outside the structure completely, the pumping action is not effective and there are no bona fide clones. In some cases, one can see clonelike pulses, but they are highly distorted and at low amplitude. Additionally, if the pumping pulses are too wide, one violates the $\tau_p \ll \tau_s$ condition and can then obtain very large but severely distorted output pulses.

Figure 6 shows the effect of pumping pulse power on the signal and clone output response. The operating parameters were the same as for Fig. 5, except for small changes in the pumping pulse timing. Figure 6(a) shows three output power vs time traces in the same format as Fig. 5(a), but for a sequence of P_{pump} levels, as indicated. The vertical axis shows normalized power levels that are scaled to the peak value for the $C1'$ pulse for $P_{\text{pump}}=19.1$ W. Figure 6(b) shows P_{peak} vs P_{pump} for the pulses in Fig. 6(a), as indicated. The vertical lines mark the specific P_{pump} values used in Fig. 6(a). The lower limit of 1 nW for the vertical axis in Fig. 6(b) represents the noise floor for the observation of clones. The lines shown simply connect the points.

One noteworthy aspect of the data in Fig. 6 is that the expeditious choice of the pumping pulse power and timing allows one to produce sequences of pulses that decrease, are equal, or increase in amplitude. Figure 6(b) shows a special situation for which the P_{peak} vs P_{pump} response curves all cross at about the same point. This realization of a common

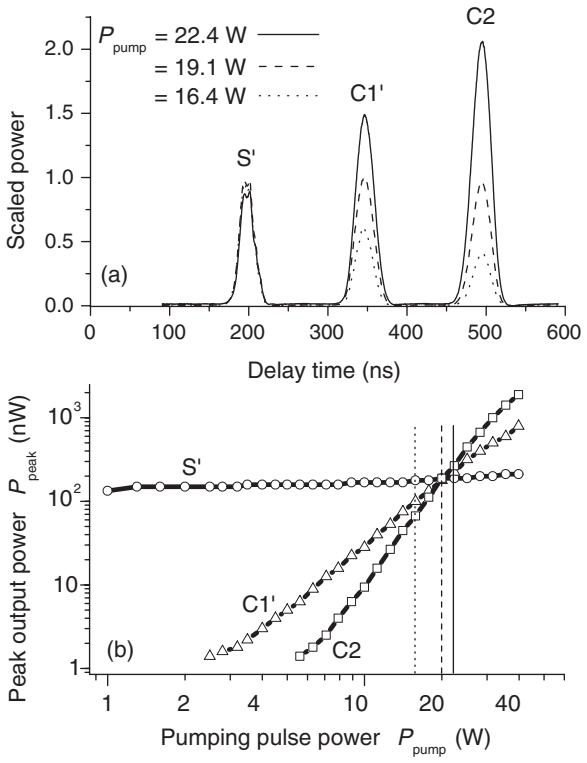

FIG. 6. Signal and clone output response and output pulse peak powers as a function of pumping pulse power. (a) shows signal power vs time traces for the signal pulse S' and the two clone pulses $C1'$ and $C2$ for three different pumping powers (P_{pump}), as indicated. (b) shows output pulse peak power P_{peak} vs P_{pump} for these pulses. The vertical lines in (b) mark the P_{pump} values for the three sets of profiles in (a).

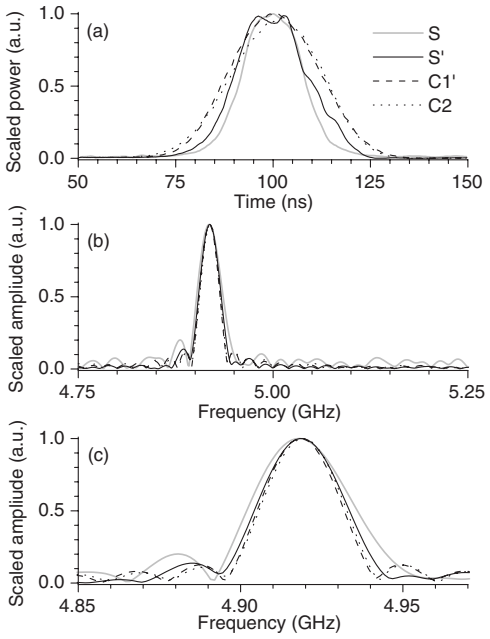

FIG. 7. The input pulse S, the three equal-amplitude output pulses from Fig. 6(a), and the Fourier transforms of those pulses, for comparison. (a) shows the power vs time traces for the input pulse S and the three for the equal-amplitude pulses in Fig. 6(a), for P_{pump}=19.1 W, overlapped on an expanded time scale. (b) shows the Fourier transforms of the pulses in (a). (c) simply shows the data in (b) on an expanded scale. All three graphs use the same legend. The data were obtained by sampling the pulses.

crossover point was accomplished through a careful adjustment of the initial signal pulse power and the timing and widths of the pumping pulses. Small changes in either parameter can serve to shift the individual crossover points up or down, and to the left or right. The pumping pulse timing also can affect the slopes of the individual responses.

Overall, Fig. 6 demonstrates the ability to control the relative sizes of the output pulses through changes in P_{pump}. There are three specific points of note. First, both graphs show that the P_{peak} for S', not S, is essentially independent of P_{pump}. The overall rate of change in P_{peak} with P_{pump} for the S' data in Fig. 6(b) is about 2 nW/W. This weak response is attributed to the short duration of the pumping pulse. Previous work[6–9,11] has shown that parametric pumping pulses of the same sort as used here can produce substantial amplification for both linear and nonlinear signal pulses. In these experiments, however, the pumping pulses were wide, on the order of 15 to 30 ns. In the current cloning experiments, *narrow* pumping pulses, with a duration τ_p that is much shorter than the signal pulse width τ_s, are required in order to obtain clean reversed idle pulses. Wide pumping pulses, therefore, are precluded.

Second, both graphs also show that this rate of change, taken as A, is larger for the second clone $C2$, relative to the first clone $C1'$. The A values for the $C1'$ and $C2$ data in Fig. 6(b) are about 21 and 55 nW/W, respectively. This more than a factor of 2 increase in A for the $C2$ clone, relative to the $C1'$ clone, is likely due to the fact that $C2$ experiences more pumping pulses and different sequences of pumping processes than does $C1'$. Keep in mind that the overall output pulse height depends on the pumping efficiencies at different points inside the pumping region, possibly different pumping amplification factors for forward and reverse processes, and normal pulse decay.

Third, Fig. 6(b) shows that a higher P_{pump} is needed to produce an observable $C2$ clone, relative to the P_{pump} needed to observe a $C1'$ clone. One can see from the data at the low end of the P_{peak} axis that the $C1'$ clone emerges from the 1 nW noise floor at $P_{pump} \approx 2.5$ W, while about 5.6 W is needed to observe the $C2$ clone. This noise floor difference is primarily due to the fact that the second idle pulse had a much lower amplitude than did the initial idle pulse R from which the $C1'$ pulse was created. More pumping power was, therefore, needed to push the signal up to observable levels.

Figure 7 gives further evidence that the output pulses $C1'$ and $C2$ are clones of the original pulse S. Figure 7(a) shows the normalized S', $C1'$, and $C2$ pulses from Fig. 6(a) for P_{pump}=19.1 W, along with the corresponding signal pulse S for no pumping. The pulses are overlapped and shown on an expanded time scale to illustrate the good matchup in the pulse profiles. Pulse S is normalized to the $C1'$ pulse. The Fourier transforms of the pulses from Fig. 7(a) are shown in Fig. 7(b) in a scaled amplitude vs frequency format. Figure 7(c) simply shows the data in Fig. 7(b) on an expanded scale. All three graphs use the same legend. For the results shown,

the central 50 ns of each pulse was separately sampled, the data were zero padded, and a standard fast Fourier transform analysis was done.

Figure 7(a) show that the $C1'$ and $C2$ clone pulses both have the same shapes and nearly the same widths as S and S'. Figure 7(b) shows that the $C1'$ and $C2$ clones have the same central carrier frequency and the same spectral profile as S. The small sidebands, normally associated with square pulses, are present because of the narrow 50 ns sampling region, which serves to cut off the pulse tails. These data provide a conclusive demonstration that $C1'$ and $C2$ are, in fact, clones of S.

VI. SUMMARY AND CONCLUSIONS

In summary, sequential short parametric pumping pulses applied to a single propagating magnetostatic spin-wave pulse in a thin YIG film strip have been used to achieve spin-wave pulse trapping and cloning. The unpumped signal pulse, the parametrically pumped output pulse, and the two additional output pulses produced after a sequence of phase conjugation and parametric amplification operations, all had the same shape, the same central frequency, and the same spectral profile. The two phase-conjugated output pulses are taken, therefore, to be clones of input pulse. These two clones may also be considered trapped because they make one or more round trips with overall propagation distances of several millimeters. The peak output powers of the cloned pulses were tunable by an adjustment of P_{pump}. The results presented here could be useful for signal processing device applications, such as a microwave pulse multiplexer. Finally, the cloning and trapping technique, through fast and broadly localized parametric pumping, as demonstrated here, should be generally applicable to any medium which can support a three-wave parametric interaction.

ACKNOWLEDGMENTS

This work was supported in part by the U.S. Army Research Office, Grants No. W911NF-04-1-0247 (MURI) and No. DAAD19-02-0197, the Office of Naval Research (U.S.A.), Grant No. N00014-06-1-0889, and the Science and Technology Center in the Ukraine, Grant No. 3066.

[1] L. Salasnich, Laser Phys. **13**, 547 (2003).
[2] J. Berges and J. Serreau, Phys. Rev. Lett. **91**, 111601 (2003).
[3] Y. Guan, J. W. Haus, and P. Powers, J. Opt. Soc. Am. B **21**, 1225 (2004).
[4] V. Komine, S. Galliou, and A. Makarov, IEEE Trans. Ultrason. Ferroelectr. Freq. Control **50**, 1656 (2003).
[5] J. T. Mendonça, A. Serbeto, R. Bingham, and P. K. Shukla, J. Plasma Phys. **71**, 119 (2005).
[6] G. A. Melkov, Y. V. Kobljanskyj, V. I. Vasyuchka, A. V. Chumak, and A. N. Slavin, IEEE Trans. Magn. **40**, 2814 (2004).
[7] G. A. Melkov, A. A. Serga, V. S. Tiberkevich, A. N. Oliynyk, A. V. Bagada, and A. N. Slavin, IEEE Trans. Magn. **35**, 3157 (1999).
[8] D. D. Stancil, *Theory of Magnetostatic Waves* (Springer, New York, 1993).
[9] G. A. Melkov, Y. V. Kobljanskyj, A. N. Slavin, and V. S. Tiberkevich, Radiotekh. Elektron. (Moscow) **48**, 135 (2003) [J. Commun. Technol. Electron. **48**, 119 (2003)].
[10] J. M. Nash, C. E. Patton, and P. Kabos, Phys. Rev. B **51**, 15079 (1995).
[11] P. A. Kolodin, P. Kabos, C. E. Patton, B. A. Kalinikos, N. G. Kovshikov, and M. P. Kostylev, Phys. Rev. Lett. **80**, 1976 (1998).